STUDY ON THE CHARACTERISTICS OF SAND AND WIND FLOW OF A NEW TYPE OF SAND BARRIER BASED ON NUMERICAL SIMULATION AND EXPERIMENT

/

基于数值模拟和实验的新型沙障的风沙流特征研究

Sibin ZHANG, Weiqiang ZHENG*), Liping ZHANG
[1)]College of Mechanical Engineering, Xinjiang University, Urumqi 830046 / China
Tel: +86-18384082033; E-mail: xjzwq@xju.edu.cn
DOI: https://doi.org/10.35633/inmateh-76-94

Keywords: *Numerical simulation, agricultural security, new sand barrier, windproof efficiency, field experiment, wind-blown sand*

ABSTRACT

The natural conditions in northwestern China are extremely harsh, with severe desertification. Frequent sandstorms cause significant damage to transportation infrastructure along desert margins, agricultural cash crops, and the local ecological environment. This study proposes a novel high vertical curved sand barrier system. Field experiments were conducted to validate numerical simulation results, and the properties of wind-driven sand movement and protective efficiency of these barriers were analyzed. Furthermore, double-row sand barriers with varying spacing were investigated to determine the optimal arrangement. The research demonstrates that the flow deflection angle of the high vertical curved sand barrier relative to the vertical direction significantly impacts its protective efficiency, showing a fluctuating pattern with changing angles. When the inlet airflow speed reaches 10 m/s with a barrier inclination angle of 75°, the leeward deceleration zone achieves an area of 25.450 m² with a coverage range of 19.31H (where H represents barrier height), resulting in optimal overall protective efficiency. For double-row sand barriers, the protective efficiency is influenced by inter-barrier spacing. As the spacing between two rows increases, the protective efficiency initially improves before declining. The system reaches peak overall protective efficiency when the inter-barrier spacing is set at 20H.

摘要

中国西北地区的自然条件恶劣，荒漠化较为严重。沙尘暴天气频发，对沙漠边缘交通设施、农业经济作物和当地生态环境造成破坏。本文提出一种新型高立式曲线沙障，通过野外实验验证了数值模拟结果，并分析了高立式曲线沙障的风沙流特征和防护效率。对不同间距下的双排沙障进行研究，得出最优铺设间距。研究表明，高立式曲线沙障相对于垂直方向的角度显著影响新型沙障的防护效率，其防护效率随着角度的改变呈现波动格局。当入口风速为 10m/s，沙障倾斜角度为 75°时，沙障后方的减速区面积达到 25.450 m²，覆盖范围为 19.31H，沙障整体防护效率最佳。双排沙障的防护效率受到沙障间距的影响，随着两排沙障间距的增强，防护效率先增加后减小。当两排沙障间距达到 20H 时，沙障整体防护效率最优。

INTRODUCTION

Desertification is a critical global ecological issue that significantly impacts human survival and development. According to UNCCD assessments, China is classified among the top-tier countries most severely impacted by desertification on a global scale, with its northwestern region being particularly vulnerable due to harsh natural conditions and scarce land resources, making it a typical example of an ecologically fragile zone (*Yifei C. et al., 2024*). Xinjiang is the largest province in China's northwest region and the area most severely affected by desertification, with the greatest expanse of desertified land in the country. It has long been influenced by the westerlies, the Siberian High, and a continental arid climate (*Bingqi Z. et al., 2014*). The sandstorms carry massive amounts of sand particles that can bury vast areas of farmland. Through sand burial, wind erosion, and windblown sand attacks, they cause ecological degradation and significant losses to people's lives and property (*Chuijie W. et al., 2008*).

Desertification control interventions are primarily functionally partitioned into mechanical sand control and biological sand control. Sand control projects can protect local desert vegetation and farmlands, and prevent further expansion of desertification. Among desertification control measures, engineering measures address the symptoms, while biological measures tackle the root causes.

The systematic integration of both engineering and biological measures offers a fundamental solution for effective wind and sand control (*Muning Z. et al., 2006; Jianjun Y., 2007*).

Mechanical sand control measures demonstrate faster effectiveness compared to biological approaches. By altering underlying surface properties and increasing ground roughness, mechanical sand barriers effectively reduce sand flow volume and erosion intensity, thereby achieving rapid stabilization of mobile sands (*Jing S. et al., 2023*).

Straw checkerboard barriers constitute the canonical aeolian sand control infrastructure, demonstrating maximum implementation density along desertification fronts worldwide. It plays an irreplaceable role in wind prevention and sand fixation, precipitation interception, reduction of water evaporation, and nutrient provision for sandy soil (*Jiayuan D. and Xiangyun Q., 2019*).

The direct effect of straw checkerboard sand barriers is to increase surface roughness. Sand particles tend to accumulate around the barriers, promoting the formation of concave surfaces (*Na Z. et al., 2014; Xiaohong D., 2015*). *Li L. and Tianli B., (2015*), conducted experimental and numerical studies on the design of checkerboard sand barriers for desertification control projects. Field observation results demonstrated that the installation of checkerboard barriers induces substantial airflow deceleration behind sand dunes. The size and shape of straw checkerboard sand barriers significantly influence sand flow patterns and near-surface wind speed distribution (*Ze M. et al., 2024; Jianjun Qet et al., 2007; Kecun Zet et al., 2012; Chunlai Zet et al., 2016*).

The installation of straw checkerboard sand barriers gradually alters the surface aeolian sand structure, effectively inhibiting sand drift and playing a vital role in local ecological restoration (*Yanfu Let et al., 2017; Yuqiu G. et al., 2004*).

For critical windproof and sand-blocking areas such as railways, highways, and farmland, high vertical sand barriers demonstrate excellent wind and sand control effectiveness. *Cheng X et al., (2021),* conducted field studies on the windproof and sand-blocking characteristics of high vertical nylon net sand barriers. Under low wind speed conditions (below 12 m/s), the effective protection distance was measured at 3H (where H represents the barrier height) for single-row barriers, while double-row barriers exhibited a leeward protection zone extending to 12H. The windproof fence barrier induces measurable velocity attenuation across the 100-220 meters behind the barrier, but it has no significant impact on the overall airflow distribution (*Jianhua X. et al., 2022; Tao W. et al., 2018*). *Li Kaichong et al., (2017),* examined the influence of aperture configuration on the sand-blocking efficiency of sand barriers. When the wall aperture angle was set at 135°, both the accumulated sand volume and the barrier's sand-blocking efficiency reached their optimal levels. *Chen Boyu et al., (2019),* investigated perforated sand fences with different aperture sizes and found that the variation in aperture diameter is a key parameter affecting the flow acceleration domain, the length of the leeward vortex region, and the distribution of surrounding sediments. *Zhang Kai et al., (2021),* conducted indoor wind tunnel experiments to analyze the flow field characteristics, porosity, and sand-blocking effectiveness of single-row vertical sand barriers made of HDPE panels. The results indicated that the sand-blocking efficiency of a single-row HDPE barrier was lower than that of multi-row sand barriers. *Wang Fang et al., (2023),* conducted numerical simulations using Fluent software to analyze the spacing and height of double-row sand barriers. The results revealed a positive correlation between barrier height and protective performance. Optimal windproof efficiency was achieved when the barrier height ranged between 1.5~2 m with a spacing of 2H (where H represents the barrier height).

In summary, scholars worldwide have conducted extensive research on the windproof and sand-blocking performance and mechanisms of sand barriers, accumulating substantial technical and engineering application experience. Low vertical barriers such as straw checkerboards can be deployed over large areas to effectively increase surface roughness and prevent desertification erosion. However, such barriers require long-term ecological restoration and cannot immediately establish effective wind and sand control for farmlands, railways, and highways at desert margins. In areas with severe wind-sand hazards, tall vertical barriers can effectively block sand-laden winds below the barrier height while creating a deceleration zone behind the barrier, thereby providing timely protection for desert highways, railways, and ecological farmlands against wind-sand damage.

Therefore, this study focuses on a novel tall vertical curved sand barrier as the research subject. Through numerical simulation methods complemented by field experiments to validate the simulation results, the protective efficiency of the curved sand barrier under various parameters was systematically investigated. The findings aim to provide theoretical design foundations for windproof and sand-control projects in regions severely affected by wind-sand hazards.

MATERIAL AND METHODS

Description of the study area

As shown in Figure 1, the study area is located in Nanhuzi Sand Hill next to the S235 highway in Yizhou District, Hami City, Xinjiang Uygur Autonomous Region, geographically situated at longitude 93°12'9.137" East and latitude 42°29'27.028" North. The study area is rich in sand sources, with frequent sandstorms, and the wind direction of sand initiation is mostly SE and SW winds. The area has a variety of sand dunes and is characterized by a typical temperate continental arid climate. The climate is dry, with annual precipitation below 30 mm and evaporation exceeding 3,000 mm; the mean temperature is 5.0°C; the soil is typical wind-sand soil, and the vegetation is basically absent. The experimental area was artificially leveled in the early stage, and the terrain is relatively flat and open with little human traffic, making it an ideal location for observing sand prevention measures.

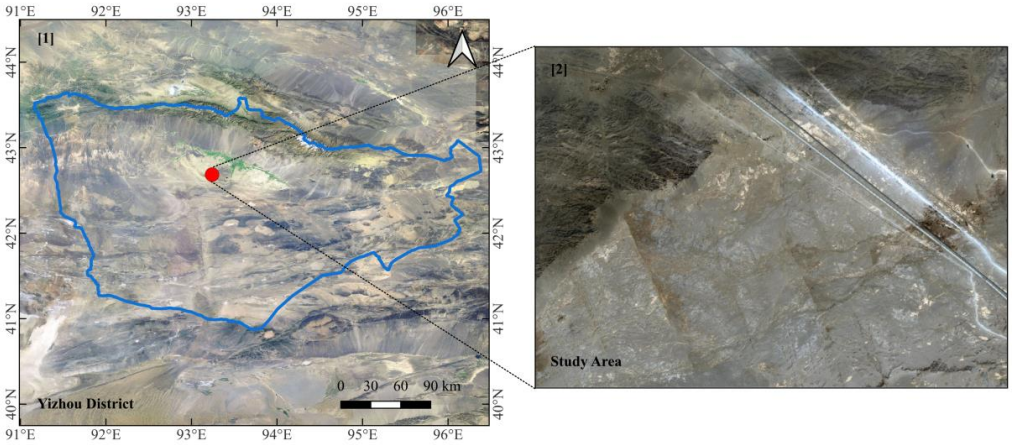

Fig. 1 - Map of the study area in the sandy hills of Nanhuzi, Hami, China

Numerical simulation

Geometric modelling and meshing

In natural environments, there exists a three-dimensional coupled wind-sand field. Theoretically, larger simulation domains allow for more complete airflow development, thereby reducing errors caused by vortices and airflow deflection around sand barriers. However, considering practical working conditions, sand particle motion is primarily governed by three forces: fluid drag force, lift force, and particle gravity. Under the action of airflow, these forces usually act within the same plane, so it is permissible to solve the problem as a two-dimensional problem (*Yan W et al., 2024*).

The computational domain of this study has a length of 60 m and a height of 12 m, as shown in Figure 2a. The height of the tall curved sand barrier is 1 m, the radius is 0.2 m, and the thickness is 0.02 m. The entrance is 12 m away from the sand barrier, and the speed exit is 48 m away from the sand barrier. The size of the flow field is consistent with the field experiment. The railway is located 48 m behind the sand barrier, and the height is set at 12 m, which is conducive to observing the airflow distribution above the sand barrier. An unstructured grid method was employed to divide the domain into triangular meshes. As shown in Figure 2b, a triangular element type was employed with approximately 600,000 elements. The grid skewness is less than 0.85, meeting the criteria for numerical simulation.

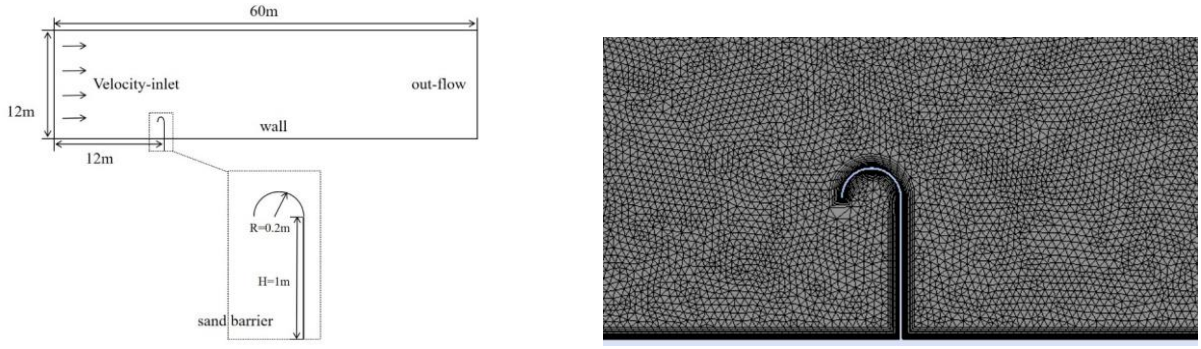

a) b)

Fig. 2 - Numerical simulation model diagram

a) Calculate regional distribution map; b) Grid partitioning diagram

Theoretical governing equation

The standard k-ε turbulence model was used to simulate the wind field, providing more accurate results for flows with significant streamline curvature and offering higher computational precision (*Bailiang Land and Douglas J.S., 2015*). The Eulerian model (two-fluid model) was selected for the multiphase flow simulation, which treats both the continuous and discrete phases as continua. It establishes continuity and momentum equations for each phase and solves them through coupled calculations of pressure and interphase exchange coefficients. The SIMPLE algorithm was then employed to solve for pressure and velocity (*Guowei X. et al., 2021; Lzael A.L. et al., 2020*).

The following equation represents the windproof efficiency:

$$\mathbf{f_{xz}} = \frac{\mathbf{v_{xz}} - \acute{\mathbf{v}}_{\mathbf{xz}}}{\acute{\mathbf{v}}_{\mathbf{xz}}} \times \mathbf{100}\% \quad (\mathbf{1})$$

where: $\mathbf{f_{xz}}$ is wind protection efficiency; x is the distance from the sand barriers; z is the height above ground level (expressed as a multiple of the height of the sand barriers); $\acute{\mathbf{v}}_{\mathbf{xz}}$ is the wind speed relative to the wall surface under sand barrier protection; $\mathbf{v_{xz}}$ is the wind speed relative to the wall surface without sand barrier protection (*Yana L. et al, 2025; Jing S. et al, 2024*).

The following equation shows the retention rate of sand particles:

$$\boldsymbol{n} = \frac{\mathbf{W} - \mathbf{Q}}{\mathbf{W}} \times \mathbf{100}\% \quad (\mathbf{2})$$

where: **n** is the sand barrier retention rate; **W** is the amount of sand transported in the wilderness for the same wind speed and altitude (g·cm^{-2}·min^{-1}); **Q** is the sand transport flux of sand particles behind the sand barrier (g·cm^{-2}·min^{-1}).

Calculated parameter

Boundary conditions for numerical simulation: the left side is a velocity inlet (constant), the right side is an outlet (free outflow), the bottom is a wall, and the top is a symmetry plane (*Yang D. et al., 2021; Ascanio D.A. et al., 2013*). as detailed in Table 1.

Table 1

Numerical simulation of calculated parameters

Variable	Parameters	Variable	Parameters
Air density/(kg·m^3)	1.225	Sand diameter/m	1×10^{-4}
Air viscosity/Pa·s	1.7894×10^{-5}	Sand viscosity/(kg/m·s)	0.047
Turbulence intensity	0.05	Sand Volume fraction/%	0.02
Temperature/K	256.95	Sand density/(kg·m^3)	2650
Mach number	<0.3	Convergence criteria	<10^{-5}

Field experiment design

As shown in Figure 3, the sand barriers used in this experiment were fabricated with PLA material at a 2:1 scale reduction to verify the windproof and sand-blocking performance of barriers with a 75° inclination angle. The actual height of the sand barrier is 0.6 m, and its width is 0.5 m. Field experimental equipment included a sand trap, an electronic balance (0.01 g precision), calipers (1 mm precision), and an anemometer (0.1 m/s precision).

To obtain accurate wind speed data, the research team collected nearly one year of local environmental data through online databases and conducted on-site wind measurements from May 6 to May 9, 2025. Wind speed measurements were taken using a smart anemometer at heights of 10 cm, 30 cm, and 50 cm. The measurement protocol involved 10 readings per hour over 5-hour periods each day for three consecutive days, with the final wind speed averages calculated from this dataset.

The measurement results showed average wind speeds of 7 m/s (range: 3-10 m/s) at 10 cm height, 10m/s (range: 5-14 m/s) at 30 cm height, and 15 m/s (range: 6-20 m/s) at 50 cm height. The data analysis revealed that wind speed variations were not significant below 30 cm height, where low wind speeds occurred more frequently, while noticeable wind speed fluctuations were observed at the 50 cm height.

The sand trap employed was a stepped collector with four height layers. Measurements revealed the following average aeolian sand transport fluxes in open terrain: 3.91 g·cm^{-2}·min^{-1} at 0-10 cm height, 2.82 g cm^{-2}·min^{-1} at 10-20 cm height, 1.41 g cm^{-2}·min^{-1} at 20-30 cm height, and 0.53 g cm^{-2}·min^{-1} at 30-40 cm height. Figure 3 shows the on-site installation layout of the sand barriers.

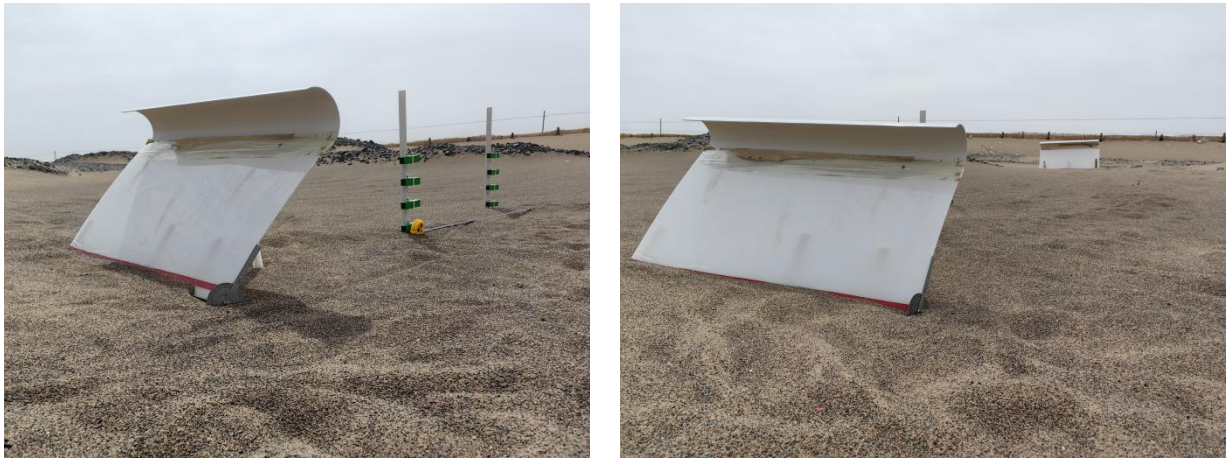

a) b)

Fig. 3 - Sand barrier layout diagram

a) Single-row sand barrier; b) Double-row sand barriers

RESULTS

- **Numerical simulation results and analysis**

The influence of sand barrier inclination angle on windproof effectiveness

Figure 4 shows the wind velocity contour plots of sand barriers with five different inclination angles under an incident flow velocity of 10 m/s. Specifically: Figure 4a displays the wind velocity contour for a 90° inclination angle, Figure 4b for 75°, Figure 4c for 60°, Figure 4d for 45°, and Figure 4e for 30°.

As illustrated in Figure 4, the novel sand barrier exhibits a wind velocity distribution pattern similar to vertical sand barriers. When airflow encounters the barrier, it obstructs the approaching wind, creating three distinct zones: small deceleration zones are formed on the windward side of the sand barrier, acceleration zones are formed at the top of the sand barrier, and turbulence zones are formed on the leeward side of the sand barrier. The innovative design of this sand barrier prevents direct perpendicular wind force. Notably, variations in the barrier's inclination angle dynamically modify the spatial dimensions of both the crest acceleration zone and the leeward deceleration zone.

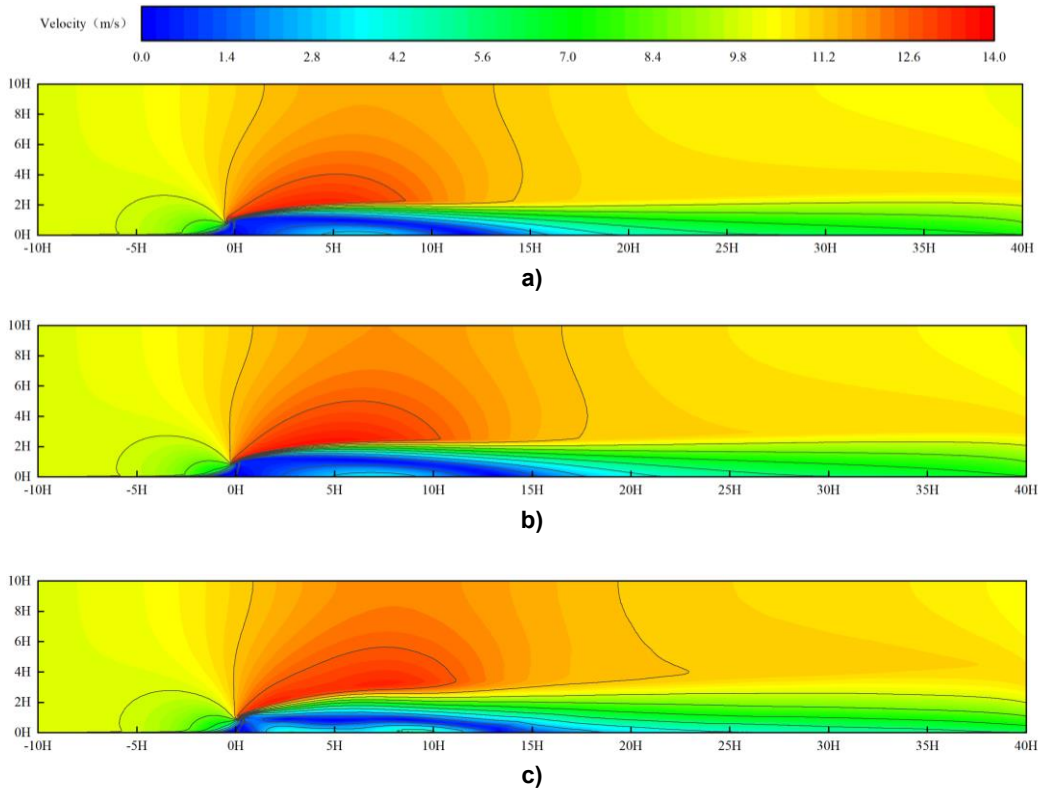

a)

b)

c)

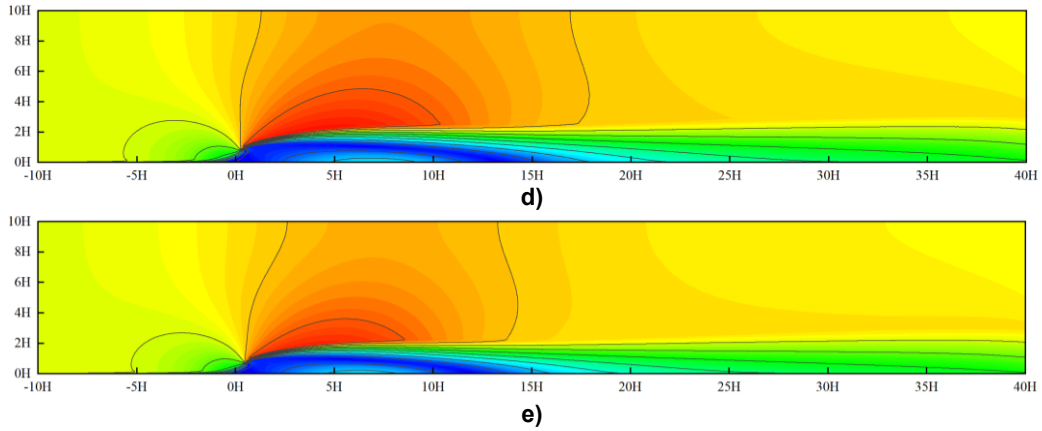

Fig. 4 - Airflow velocity contour of single-row sand barrier

a) α=90°; b) α=75°; c) α=60°; d) α=45°; e) α=30°

A comparative analysis of sand barriers with different inclination angles in Figure 4 was conducted using 2.5 m/s as the minimum threshold wind speed for sand particle entrainment. The areas with wind speeds below 2.5 m/s for barriers inclined at 90° to 30° measured 21.515m^2, 25.450m^2, 17.332m^2, 24.299m^2, and 19.039m^2 respectively. The protective area of the turbulent zone behind the barriers exhibited an initial increase followed by a decreasing trend. The horizontal coverage ranges of the 2.5 m/s wind speed contour behind the sand barriers were 17.51H, 19.31H, 19.64H, 19.03H, and 17.49H, respectively. The size of the deceleration zone generally showed an initial increase followed by a decreasing trend. Overall, the 75° inclined sand barrier demonstrated better protective effectiveness under 10 m/s wind conditions.

Flow field patterns around sand barriers

Figure 5 shows the horizontal wind speed distribution characteristics around the new sand barrier at different inclination angles. Figures 5a to 5d show the horizontal wind speed diagrams at heights of 0.2H, 0.5H, 1H, and 3H above ground level.

At heights of 0.2H and 0.5H above ground level, the horizontal velocity variation demonstrates an initial decrease followed by an increase, exhibiting an approximately "W"-shaped distribution along the distance. Due to the effect of sand barriers blocking airflow, the airflow velocity decreases sharply in front of the barrier. In the leeward region, the combined effects of low pressure and turbulence cause the velocity to first increase and then decrease. As the distance between the airflow and the sand barrier increases, the wind speed behind the sand barrier gradually recovers. Below the barrier height (1H), the wind speeds behind sand barriers with inclination angles from 90° to 30° are reduced to 6.09 m/s, 5.70 m/s, 5.79 m/s, 6.06 m/s, and 6.52 m/s, respectively. These results indicate that at a 75° inclination angle, the airflow velocity is lowest under 10 m/s wind conditions, demonstrating optimal protective effectiveness.

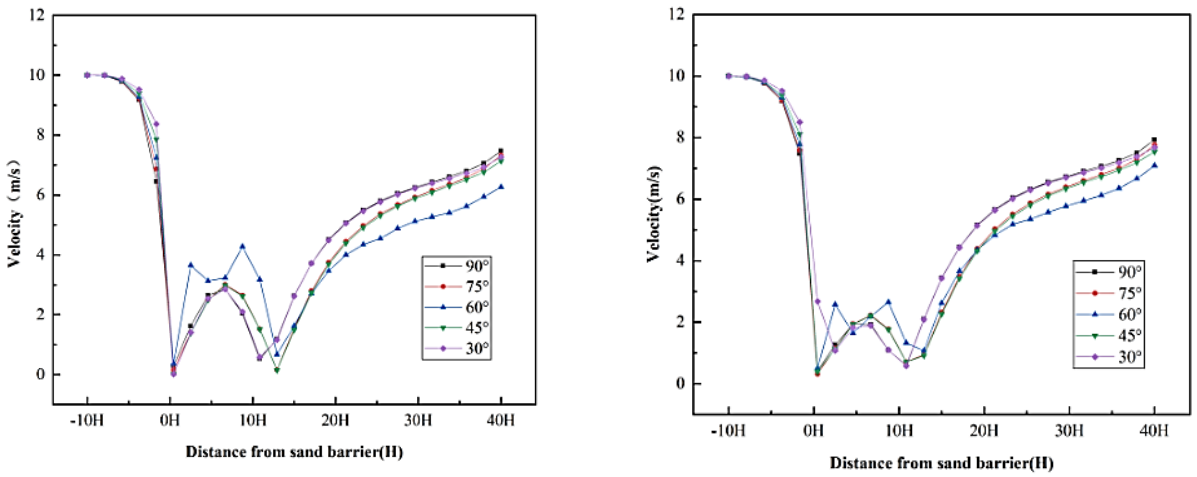

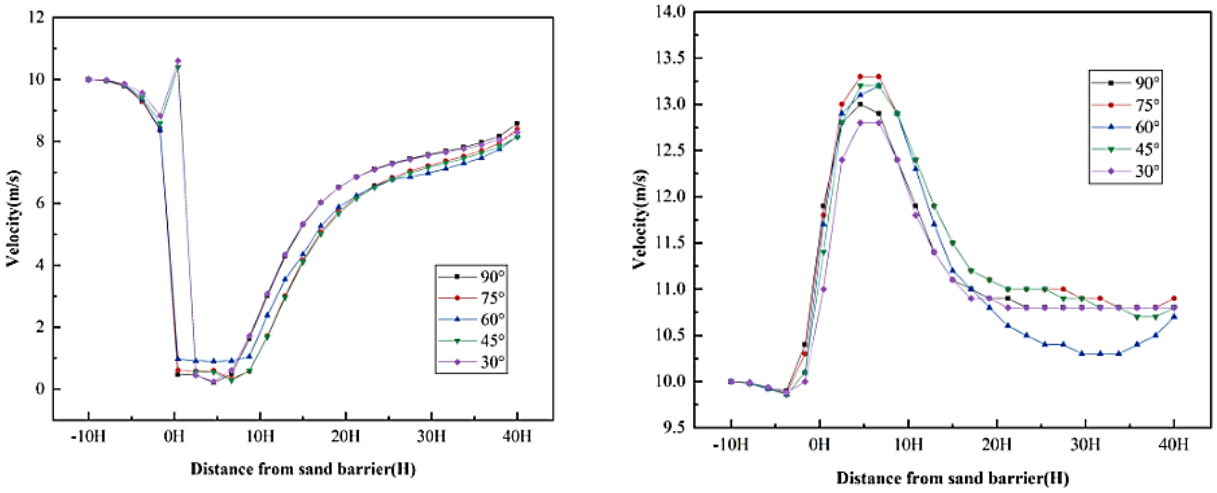

Fig. 5 - Planar wind speed profiles for differently inclined sand barriers

a) D =0.2H; b) D =0.5H; c) D =1H; d) D=3H

Figure 5d demonstrates that the velocity variation at 3H height above ground follows the same pattern as observed at the other three elevations, exhibiting an inverted "V"-shaped distribution characteristic. This indicates that the windproof is less effective at a height of 3H and that the protective height of the windproof is lower than its own height.

Figure 6 presents the vertical wind speed characteristics around the novel sand barriers at different inclination angles.

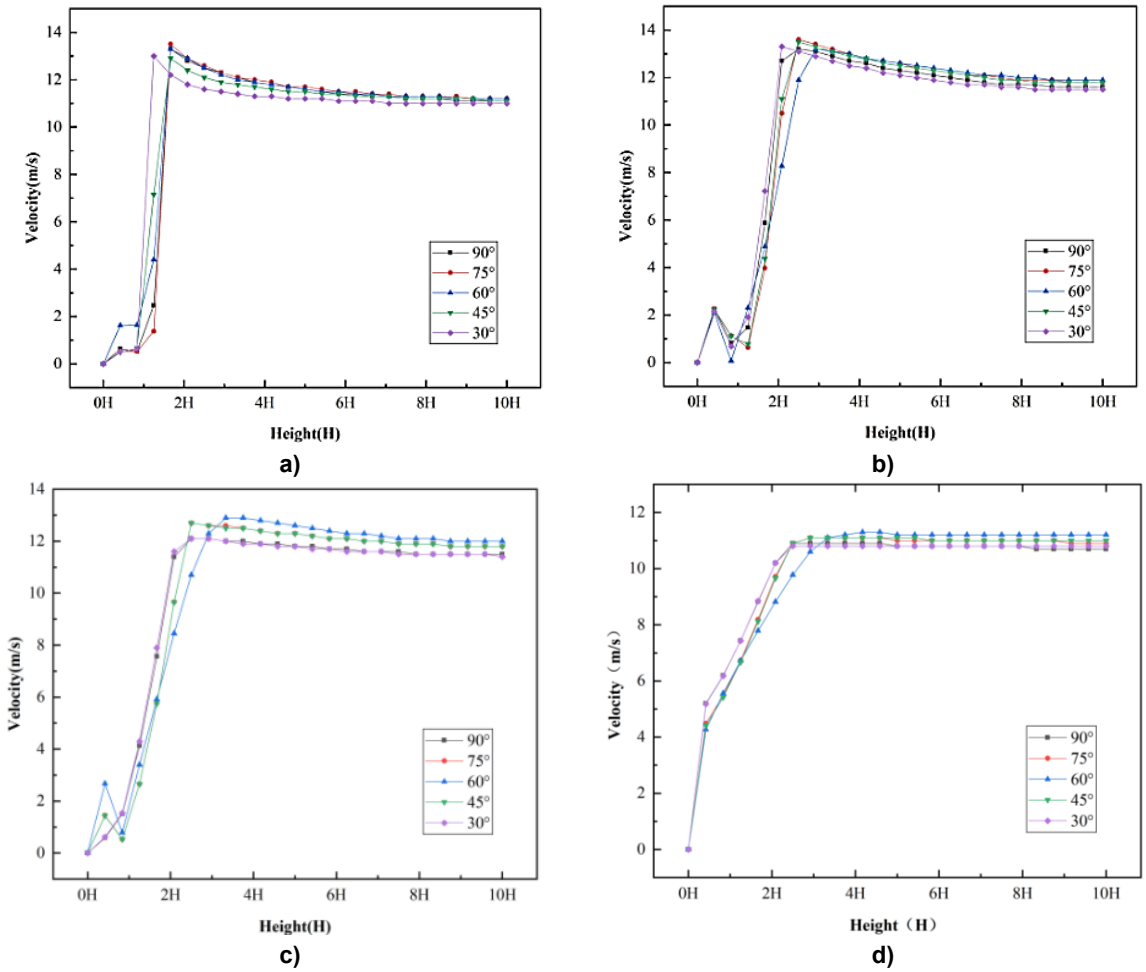

Fig. 6 - Vertical velocity distribution patterns for variably inclined sand barriers

a) D=1H; b) D =5H; c) D =10H; d) D =20H

Figures 6a to 6d display the vertical wind speeds at distances of 1H, 5H, 10H, and 20H from the barriers. The sand barrier exhibits similar wind speed variation patterns at 1H, 5H, 10H, and 20H distances, though the variation trends are significantly influenced by elevation height. Below the height of 1H, wind speed first increases and then decreases as the height above ground increases; between the heights of 1H and 2H, the wind speed gradually increases, the wind protection effect decreases, and it enters into the acceleration zone. When the height above the ground exceeds 2H, the wind-blocking effect of the sand barriers on the incoming wind decreases, and the airflow behind the barriers comes into contact with the external airflow, so that the wind speed gradually tends to stabilize.

Windproof efficiency variation patterns of sand barriers

Figure 7 selects wind speeds at four heights: 0.2H, 0.5H, 1H, and 3H above the ground. Based on the windproof efficiency formula (1), the windproof efficiency of sand barriers at different tilt angles is calculated, with the overall distribution trend showing an "M" shape. At three heights: 0.2H, 0.5H, and 1H, the windproof efficiency first increases and then decreases, indicating that the main protective range of the sand barriers is in the area below the height of the barriers. At a height of 3H, the sand barrier has no effect on blocking airflow, so the windproof efficiency becomes negative. The movement of sand particles in the desert mostly occurs near the surface.

This study focuses on the analysis below the height of the sand barrier (1H). The average windproof efficiencies of sand barriers with tilt angles ranging from 90° to 45° are 39.1%, 43.0%, 42.1%, and 39.4%. Windproof efficiency fluctuates with changes in the angle of the sand barrier, increasing at first and then decreasing, reaching its optimum at 75°.

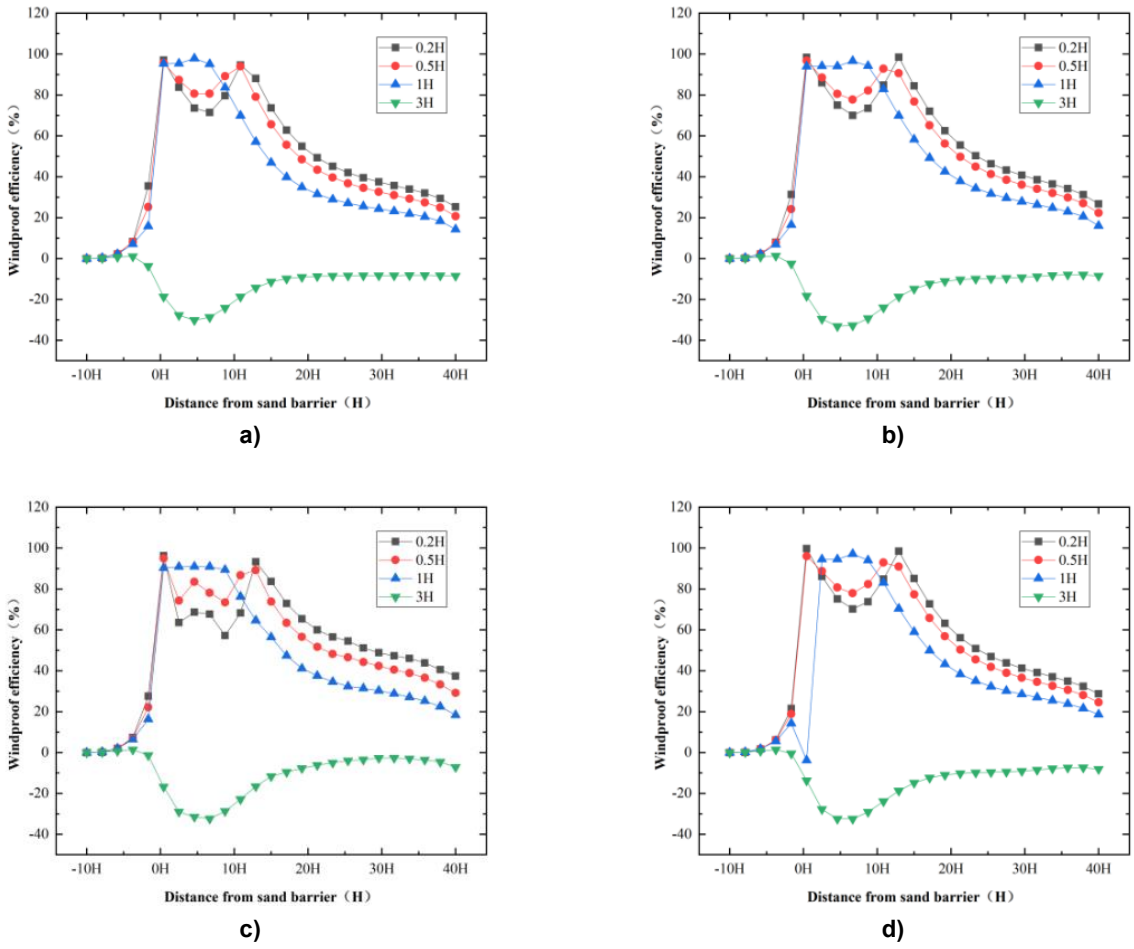

Fig. 7 - Windproof efficiency diagram of sand barriers at different tilt angles

a) α=90°; b) α=75°; c) α=60°; d) α=45°

The sediment distribution of sand barriers

Due to the significant mass difference between sand particles and air, when wind-sand flow reaches the vicinity of a sand barrier, a pressure difference is created, generating localized resistance.

This can substantially reduce the transit speed of the airflow and weaken the energy of the wind-sand flow, causing some sand particles to deposit around the sand barrier. The study on the windproof efficiency and protective distance of sand barriers shows that a tilt angle of 75° yields better results. At this angle, the volumetric distribution of sand particles in the flow field is illustrated in Figure 8. As the volume fraction of sand particles and the accumulation time increase, more sand particles are deposited around the sand barrier.

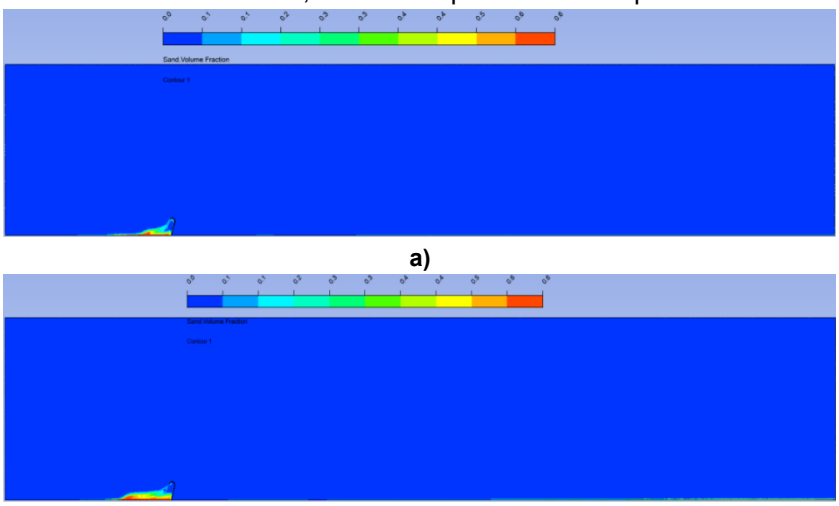

a)

b)

Fig. 8 - Contour plot of sand accumulation at the sand barrier

a) t=4s; b) t=8s

Flow distribution characteristics of double-row sand barriers

Figure 9 displays the wind speed contour plots of double-row sand barriers with spacings of 10H, 15H, 20H, and 25H at a wind speed of 10 m/s. D represents the distance between double rows of sand barriers. When the airflow reaches the first row of sand barriers, a deceleration zone forms in front of the barriers due to their blocking effect, while an acceleration zone develops above the barriers. The two rows of barriers create a vortex zone, leading to sand deposition. When the airflow reaches the second row of barriers, the wind speed is already reduced, resulting in a smaller acceleration zone. The distance between the two rows of barriers influences the overall windproof and sand-blocking effectiveness.

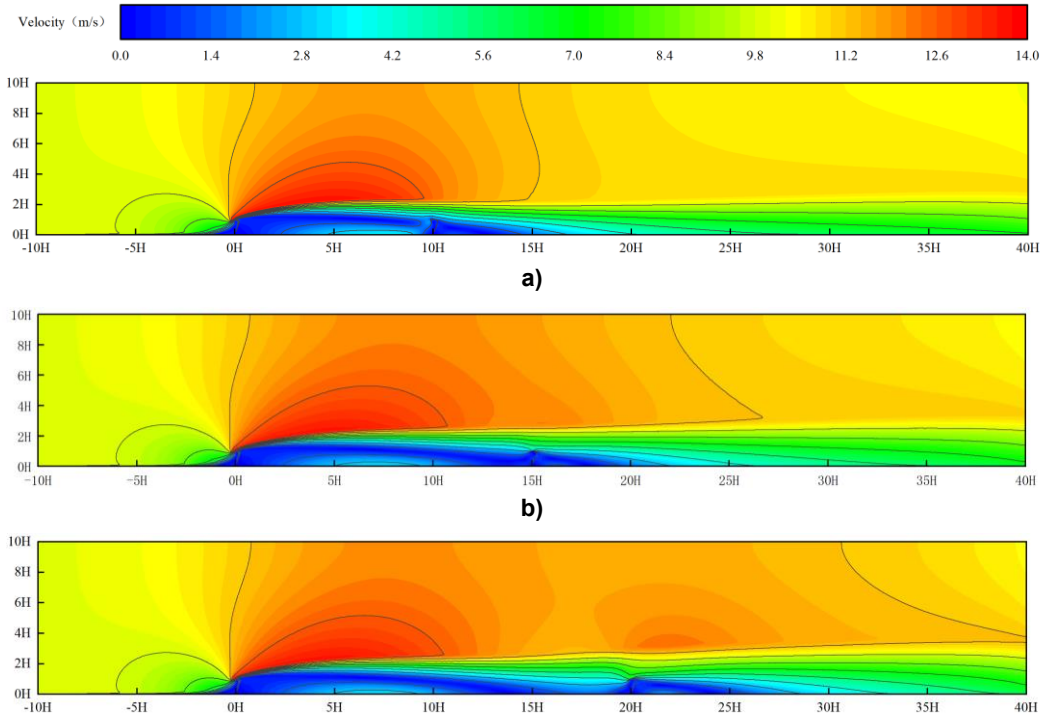

a)

b)

c)

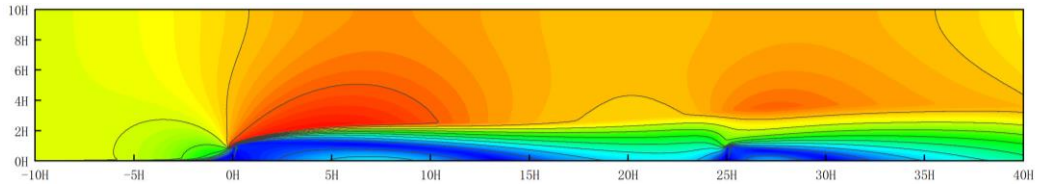

d)

Fig. 9 - Wind speed contour maps of double-row sand barriers with different spacings

a) D=10H; b) D=15H; c) D=20H; d) D=25H

The double-row sand barriers exhibit a bimodal airflow fluctuation pattern. For barriers with spacings of 10H to 25H, the areas with wind speeds below 2.5 m/s measure 22.971m^2, 31.916 m^2, 37.326m^2, and 36.693m^2, respectively. The protective area of the turbulent zone behind the barriers shows an initial increase followed by a fluctuating decrease. Overall, the double-row sand barriers with a 20H spacing demonstrate better protective effectiveness at a wind speed of 10 m/s.

Variation characteristics of windproof efficiency in double-row sand barriers

Figure 10 illustrates the windproof efficiency of double-row sand barriers with spacings of 10H, 15H, 20H, and 25H. As shown in Figures 13a~b, the overall trend of windproof efficiency for double-row sand barriers with spacings of 10H and 15H is consistent, exhibiting an initial increase followed by a decrease. From Figures 13c~d, it can be observed that the windproof efficiency for double-row sand barriers with spacings of 20H and 25H features a longer transition zone. Among sand barriers with different spacing, those with a spacing of 20H have the best overall windproof efficiency and the optimal effective protection distance.

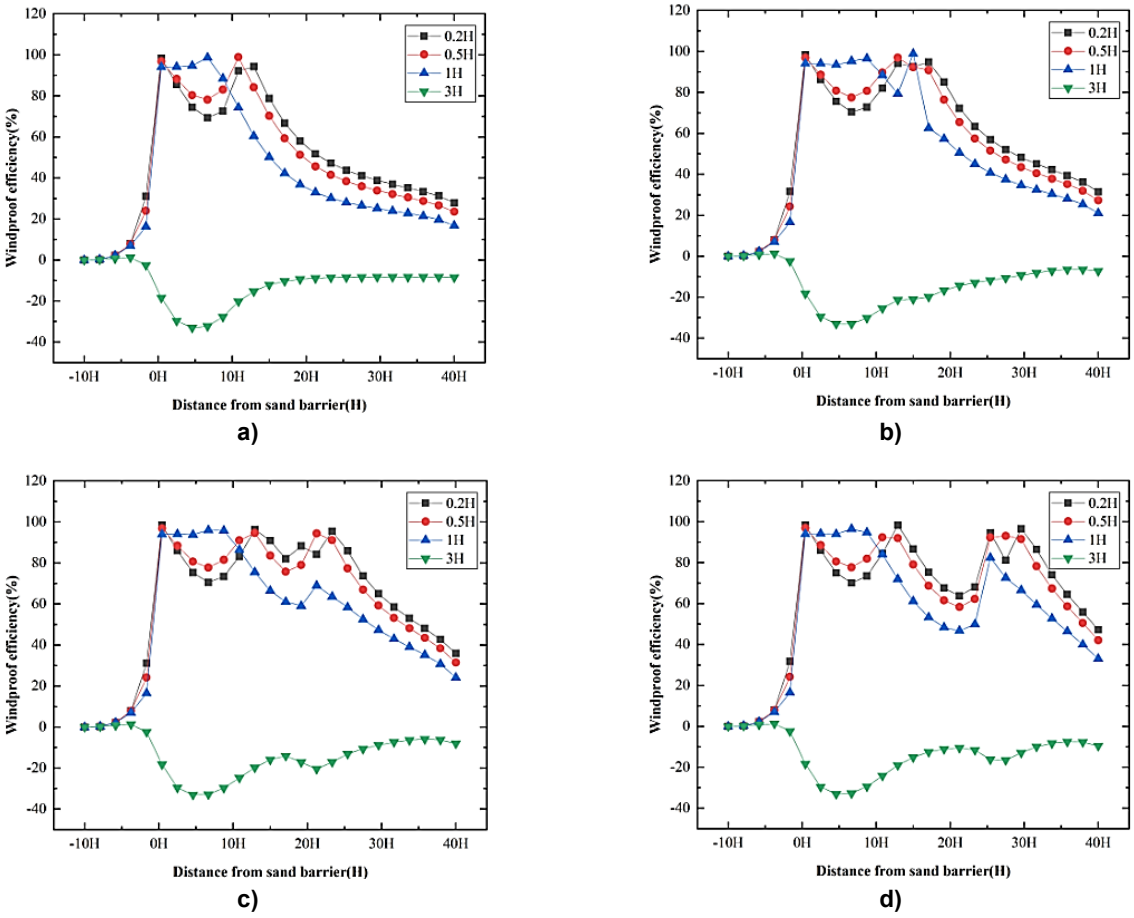

Fig. 10 - Windproof efficiency diagram of double-row sand barriers

a) D=10H; b) D=15H; c) D=20H; d) D=25H

➢ Results and analysis of field experiments

Comparative analysis of wind speed in field experiments

In field environments, wind speed variations are significant and unstable, with differences observed even at the same altitude level. Therefore, instead of directly comparing wind speed values, the windbreak efficiency is calculated using the measured wind velocity data from the open area in front of the sand barrier and the measured wind speed data behind the sand barrier. This approach allows for a more intuitive comparative analysis.

Using the 30 cm (0.5H) height layer as the comparison level, Figure 11a shows that there are certain discrepancies between the field experiment and simulation results. The maximum absolute error is 23.5%, primarily because the measurement points were located at a considerable distance from the sand barrier, and the rear measurement points were significantly affected by lateral winds, leading to a larger error. The minimum error is 4.9%, with all other errors being less than 20%. Overall, the field experiment data align well with the numerical simulation data.

As shown in Figure 11b, the maximum error is 13.6%, the minimum is 1.9%, and all other errors are less than 10%. Overall, the error distribution indicates that double-row sand barriers exhibit smaller discrepancies compared to single-row barriers and align more closely with the numerical simulation results. This further validates the reliability of numerical simulation and can accurately display the patterns of airflow.

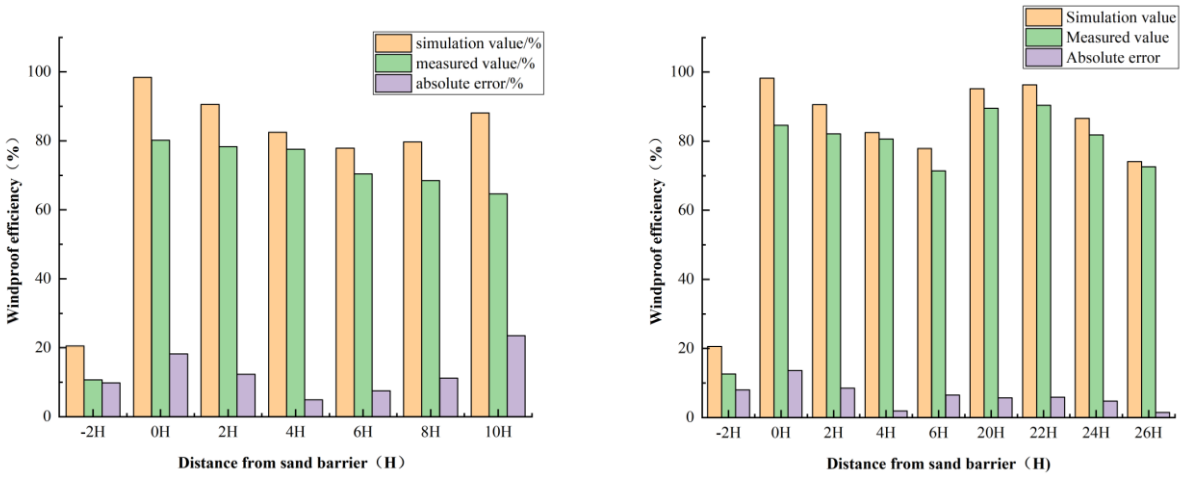

a) b)

Fig. 11 - Comparison of errors between field experiments and numerical simulations

a) Single-row sand barrier; b) Double-row sand barriers

Analysis of sand deposition in field experiments

Figure 12 shows the measurement and analysis of sand deposition in the experimental area. The main area for sand grain migration is within the 0-10 cm height span, where the sand transport flux is greatest. As the height increases, the sand transport flux decreases significantly. The average sand transport flux at a height of 0-10 cm was 3.91 g cm^{-2}·min^{-1}. For every 10 cm increase in height, the sand transport flux gradually decreases to 2.82 g cm^{-2}·min^{-1}, 1.41 g cm^{-2}·min^{-1}, and 0.53 g cm^{-2}·min^{-1}, respectively.

As shown in Figure 12a, the 0-10 cm height range is the primary zone for sand saltation, with the maximum sand particle interception rate reaching 92.83%. As the height increases, the maximum interception rate at 20 cm is 93.61%, at 30 cm it is 90.78%, and at 40 cm it is 83.01%. This further confirms that the sand transport flux weakens with increasing height, and wind-sand activity is predominantly concentrated near the ground surface.

Figure 12b shows sand particle deposition in a double row of sand barriers. Their sand-blocking characteristics are similar to those of the single-row barriers. After sand particles collide with the barriers, most of them deposit in front of the barriers, while some particles pass over them. The sand transport flux decreases with increasing distance from the barriers. Due to the blocking effect of the first row of barriers, the sand transport flux in front of the second row is significantly reduced compared to the first row. As the row number of sand barriers increases, the wind speed in the area between the double-row barriers becomes lower, making it less likely for sand particles to saltate. Overall, the double-row sand barriers exhibit better sand-blocking effectiveness.

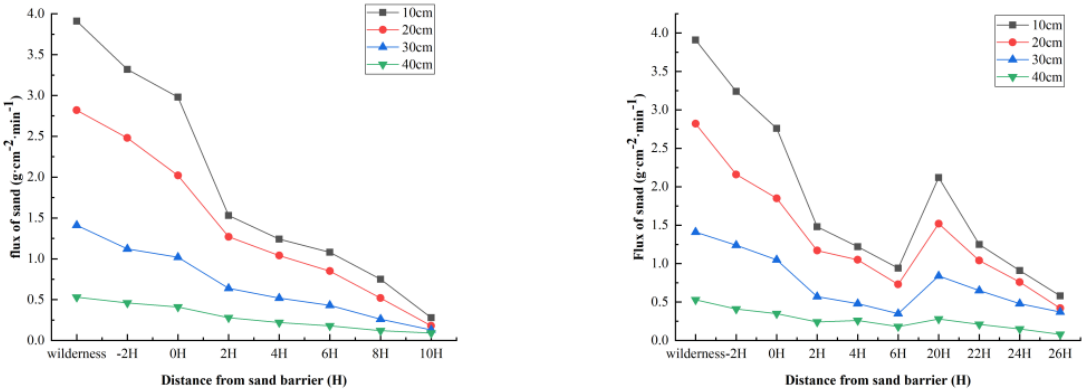

a) **b)**

Fig. 12 - Sand deposition diagrams from field experiments

a) Single-row sand barrier; b) Double-row sand barriers

CONCLUSIONS

To address the shortcomings of traditional vertical sand barriers, this study proposes a new type of curved vertical sand barrier. Using Fluent numerical simulations, the characteristics of wind-sand flow around the curved vertical sand barrier and its protective efficiency were analyzed. Finally, the results of the numerical simulation were verified through field trials, leading to the following conclusions:

1. The angle of the horizontal vertical curved sand barrier relative to the vertical direction significantly affects the protective efficiency of the new barrier. The protective efficiency of the barrier exhibits a fluctuating pattern as the angle changes. At an inlet wind speed of 10 m/s, when the barrier's tilt angle is 75°, the area of the deceleration zone behind the barrier is 25.450 m², with a coverage range of 19.31H, indicating overall better protective effectiveness. The protective efficiency begins to decline when the angle exceeds 75°.

2. The height of the vertical curved sand barrier affects the effective protection range of the sand barrier. The barrier cannot effectively intercept sand particles exceeding its height. In the vertical direction, sand particles are primarily distributed in the area below the barrier height, while in the horizontal direction, they mainly deposit in front of the barrier.

3. The overall protective efficiency of double rows of sand barriers is affected by the distance between the double rows of sand barriers. The overall protective area of double rows of sand barriers shows a fluctuating trend of first increasing and then decreasing as the distance between the sand barriers increases. When the spacing between two lines is 20H, the area with wind velocity below 2.5 m/s within the double-row barriers reaches its maximum at 37.326 m². When the spacing exceeds 20H, the overall protective area of the sand barriers begins to decrease, and the protective efficiency decreases.

Railways, highways, farmlands, and ecological restoration areas are abundant in Northwest China. Severe sandstorms can bury railways and highways under sand, reduce crop yields, and damage the local ecological environment. This study provides a solid foundation for the development of transportation infrastructure and sand prevention projects in desertification areas. Finally, the dimensions of the sand barriers can be further optimized to ensure their protective effect on agricultural areas under extreme weather conditions. Research can also be conducted on the accumulation of sand particles in front of the sand barriers to avoid affecting their effectiveness.

ACKNOWLEDGMENTS

The authors were funded for this project by the National Natural Sciences Foundation of China (NSFC), Grant/Award Number: 52265039.

REFERENCES

[1] Ascanio D.A., Eric J.R., Thorsten P., Jose S.A., Hans J.S. (2013), Numerical modeling of the wind flow over a transverse dune, *Scientific Reports*, Vol.3, pp.2858, Hangzhou/China. Fortaleza/Brazil.

[2] Bingqi Z., Jingjie Y., Xiaoguang Q., Patrick R., Yichi Z., Heigang X. (2014), Formation and evolution of sand deserts in Xinjiang, Northwest China: II. The palaeo-environmental reconstruction. *Journal of Geographical Sciences*, Vol.24(3), pp.539-559, Beijing/China.

[3] Boyu C., Jianjun C., Lingui X., Rui W., (2019), Effectiveness of hole plate-type sand barriers in reducing aeolian sediment flux: Evaluation of effect of hole size, *Aeolian Research*, Vol.38, pp.1-12, Xinjiang/China.
[4] Bailiang L., Douglas J.S., (2015), Aerodynamics and morphodynamics of sand fences: A review. *Aeolian Research*, Vol.17, pp.33-48, Suzhou/China.
[5] Chuijie W., Ming W., Liang W., (2008), Large-eddy simulation of formation of three-dimensional aeolian sand ripples in a turbulent field. *Science in China Series G: Physics, Mechanics & Astronomy*, Vol.51(8), pp.945-960, China.
[6] Chunlai Z., Qing L., Na Z., Jiaqiong Z., Liqiang K., Yaping S., Wenru J., (2016), Field observations of wind profiles and sand fluxes above the windward slope of a sand dune before and after the establishment of semi-buried straw checkerboard barriers, *Aeolian Research*, Vol.20, pp.59-70, Beijing/China.
[7] Cheng X., Hejun Z., Haibing W., Min Y., Guangpu J., (2021), Wind-proof and sand-blocking characteristics of high vertical nylon mesh sand barrier and its rational allocation (高立式尼龙网沙障防风阻沙特征及其合理配置), *Arid Zone Research*, Vol.38(3), pp.882-891, Hohhot/China.
[8] Fang W., Shixiao L., Yujia J., Weijia D., (2023), Research on the Effect of Sand Barriers on Highways in Desert Areas on Sand Control, *Sustainability*, Vol.15, pp.13906, Yinchuan/China.
[9] Guowei X., Ning H., Jie Z., Hongchao D., (2021), Investigations into the design of sand control fence for Gobi buildings, *Aeolian Research*, Vol.49, pp.100662, Lanzhou/China.
[10] Jianjun Y., (2007), Discussion on Several Problems in the Projects of Slope Ecological Protection Engineering (边坡生态防护工程中的若干问题探讨), *Research of Soil and Water Conservation*, Vol.14(5), pp.333-335, Hubei/China.
[11] Jing S., Jun W., Hailong W., Junzhe H., Shaoyun Z., (2023), Wind tunnel test study on windbreak and sand fixing effect of porous sand fixing brick grid mechanical sand barrier (多孔固沙砖机械沙障防风固沙效果的风洞试验研究), *Journal of Vibration and Shock*, Vol.42(19), pp.266-274, Zhangjiakou/China.
[12] Jiayuan D., Xiangyun Q., (2019). Application of Grass Square Sand Barrierin Windbreak and Sand Fixation (草方格沙障在防风固沙中的应用), *Construction Technology*, Vol.11(21), pp.205-207, Guangzhou/China.
[13] Jianjun Q., Ruiping Z., Kecun Z., Haiyan F., (2007), Field observations on the protective effect of semi-buried checkerboard sand barriers, *Geomorphology*, Vol.88(1-2), pp.193-200, Lanzhou/China.
[14] Jianhua X., Dongting Y., Xiaosong X., Zhengyi Y., Jianjun Q., Benli L., (2022), Numerical simulation of the airflow at the world's largest concentrated solar power plant in a desert region, *Solar Energy*, Vol.232, pp.421-432, Lanzhou/China.
[15] Jing S., Shen W., Yongzhi L., Junjie M., Junzhe H., Jun W., Pu C., Hongbo L., Boyang Z., Yong L., (2024), Experimental study on a combined sand barrier: Integration of porous mesh plate and novel porous sand-fixing bricks, *Journal of Wind Engineering & Industrial Aerodynamics*, Vol.251, pp.105809, Zhangjiakou/China.
[16] Kecun Z., Jianjun Q., Zhishan A., (2012), Characteristics of wind-blown sand and near-surface wind regime in the Tengger Desert, China, *Aeolian Research*, Vol.6, pp.83-88, Lanzhou/China.
[17] Kaichong L., Long S., Fuqiang J., Chunxiao X., Lingwei K., (2017), Research on the Relationship between Perforated Sand - blocking Wall and Sand - blocking Effect (挡沙墙开孔方式与阻沙效果的关系研究), *Journal of Railway Engineering Society*, Vol.11, pp.005-009, Lanzhou/China.
[18] Kai Z., Peiwen Z., Jianchang Z., Xingxin Z., (2021), Protective effect of multi-row HDPE board sand fences: A wind tunnel study, *International Soil and Water Conservation Research*, Vol.9(1), pp.103-115, Lanzhou/China.
[19] Li L., Tianli B., (2015), Effects of checkerboard sand barrier belt on sand transport and dune advance, *Aeolian Research*, Vol.42, pp.100546, Lanzhou/China.
[20] Lzael A.L., Eric J.R.P., Yaping S., (2020), CFD simulation of the wind field over a terrain with sand fences: Critical spacing for the wind shear velocity, *Aeolian Research*, Vol.43, pp.100574, Fortaleza/Brazil.
[21] Muning Z., Dingqiang L., Yuji Z., (2006), Study on Soil and Water Conservation Effect of Bioengineering Techniques for Slope Protection in Highway (高速公路生态护坡技术的水土保持效应研究), *Journal of Soil and Water Conservation*, Vol.21(1), pp.164-167, Guangzhou/China.

[22] Na Z., Chunlai Z., Jinlu T., Liqiang K., (2014), Flow field controlling the concave surface of the semi-buried checkerboards and its characterization by grain sizes of sediments (半隐蔽式草方格沙障凹曲面形成的流场解析及沉积表征), *Geographical Research*, Vol.33(11), pp.2145-2156, Beijing/China.

[23] Tao W., Jianjun Q., Yuquan L., Benli L., Jianhua X., (2018), Shelter effect efficacy of sand fences: A comparison of systems in a wind tunnel, *Aeolian Research*, Vol.30, pp.32-40, Lanzhou/China.

[24] Xiaohong D., Yong G., Yi Y., et al., (2015), Windproof efficiency with new biodegradable PLA sand barrier and traditional straw sand barrier (新型生物可降解 PLA 沙障与传统草方格沙障防风效益), *Journal of Beijing Forestry University*, Vol.37(3), pp.118-125, Hohhot/China.

[25] Yifei C., Feng W., Xubin P., Fangmin Z., Guoyu R., Qi L., (2024), 150-year shift of potential geographical distribution of desertification in China: Past, present and future (中国荒漠化潜在发生区域 150 年变迁:过去、现在和未来), *Chinese Science Bulletin*, Vol.69(31), pp.4637-4650, Beijing/China.

[26] Yanfu L., Zhiwei L., Zhaoyin W., Wenlong W., Yanhong J., Shimin T., (2017), Impacts of artificially planted vegetation on the ecological restoration of movable sand dunes in the Mugetan Desert, northeastern Qinghai-Tibet Plateau, *International Journal of Sediment Research*, Vol.32, pp.277-287, Nanjing/China.

[27] Yuqiu G., In-Bok L., Hideyuki S., Yong G., Guodong D., (2004), Principles of sand dune fixation with straw checkerboard technology and its effects on the environment, *Journal of Arid Environments*, Vol.53(3), pp.449-464, Beijing/China.

[28] Yang D., Shuangxi Z., Yongqi W., Tonglin Y., Jingliang D., (2021), Influence of Wind Speed, Wind Direction and Turbulence Model for Bridge Hanger: A Case Study, *Symmetry*, Vol.13, pp.1633, Hangzhou/China.

[29] Yana L., Yinxiang L., Xiaoqiang H., Quanwang Y., Daimin Y., Haijun T., (2025), Analysis of the effectiveness of four types of banded sand barriers in the Ulan Buh Desert (乌兰布和沙漠 4 种带状沙障建设成效分析), *Journal of Inner Mongolia Forestry Science & Technology*, Vol.51(1), pp.1-6, Hohhot/China.

[30] Yan W., Afang J., Jianzhou J., (2024), Numerical Simulation and Parameter Optimization of a New Slant Insertion-Opening Combination Sand Fence, *Sustainability*, Vol.16, pp.8651, Urumqi/China.

[31] Ze M., Zhongju M., Jianguo L., Alatengtaogesu., Dongying Z., (2024), Wind-prevention and Sand Fixation Effects of Checkerboard Sand Barrier Along Typical Yellow River Bank in Ulan Buh Desert (乌兰布和沙漠典型沿黄段格状沙障防风固沙效应), *Bulletin of Soil and Water Conservation*, Vol.44(2), pp.001-010, Hohhot/China.